JOURNAL OF GEOPHYSICAL RESEARCH, VOL. 90, NO. A7, PAGES 6419-6438, JULY 1, 1985

CHARACTERIZATION OF THE SOURCES OF VLF HISS AND CHORUS OBSERVED ON GEOS 1

F. Lefeuvre[1] and R. A. Helliwell

Radioscience Laboratory Stanford University, California

Abstract. Ray-tracing techniques are used to locate the apparent source regions of natural electromagnetic emissions observed on the GEOS 1 satellite and to determine the wave normal directions at this apparent source region. They are applied to VLF hiss, whose analysis in terms of the wave distribution function (WDF) has established that they often consisted of a sum of two or more very distinct wave packets at the point of observation. An example of a two-peaked WDF chorus is also examined. A two-dimensional ray-tracing program is used. For the cases analyzed here, GEOS 1 data indicate that the earth's magnetic field is to be considered as dipolar, and a diffusive equilibrium model is used to describe the medium. It is shown theoretically that even if the exact location of the source region is difficult to estimate accurately, more precise information can still be obtained on the wave normal distribution at the source region. In the examples considered, it is pointed out that the VLF hiss was generated in the vicinity of the equator at high wave normal angles.

1. Introduction

Despite many papers published on the subject, the problem of the localization of the sources of natural emissions observed within the magnetosphere is far from being completely solved. A comprehensive synthesis of the use of the measured wave data to locate the source has been recently given by Likhter (1979). We start by discussing this synthesis, and then we show how the results obtained from a wave distribution function (WDF) analysis (Lefeuvre et al., 1981) can improve our knowledge about the source of natural electromagnetic wave fields and more particularly about the sources of chorus and VLF hiss.

To locate the source, Likhter considers three type of experimental evidence: (1) the relationship between the wave frequency and the local plasma parameters at the source, (2) the enhanced probability of noise occurrence or the enhanced amplitude of the noise in particular magnetospheric regions, and (3) the relationship between the wave characteristics and other phenomena in magnetospheric plasma.

As shown by the authors quoted by Likhter, as well as by others (Burtis and Helliwell, 1976; Gurnett and Green, 1978; Calvert, 1981), the lower or upper cutoff of a natural emission may scale with one of the characteristic frequencies of the ambient plasma (electron gyrofrequency, proton gyrofrequency) defining a probable source region. However, such a relationship, when it exists, depends on the propagation characteristics between the source and the observation point.

The enhanced probability of occurrence of emissions or the enhanced amplitude of the emissions is often used to identify the sources (Russell et al., 1969; Tsurutani and Smith, 1977; Gallagher and Gurnett, 1979; etc.). However, as emphasized by Likhter, it is a reliable method in the near vicinity of the source only. Outside, particularly for ducted waves, the signal can be focused as it propagates away from the source, creating an electromagnetic field more intense than at the source (Russell et al., 1969).

In the same category of experimental evidence we include the reconstruction of frequency spectra by ray tracing from a source the characteristic parameters of which are adjusted to provide the best fit to the data (Taylor and Shawhan, 1974; Green et al., 1977). But this supposes that (1) the generation mechanism is perfectly known and (2) there is a unique position of the source to explain the set of the measured data.

The relationship between the wave characteristics (amplitude, frequency spectra) and the particle energy and pitch angle distributions is also used to locate the sources (Burton and Holzer, 1974; Tsurutani et al., 1979). However, one must be sure to compare waves and particles coming from the same interaction region, which is difficult when the waves are unducted and are observed far from the source.

Likhter does not consider the use of the wave vector orientation, arguing that the number of wave experiments with the needed aerials is still limited and that publications regarding their results are scarce. However, there is useful information on the source position based on the variation in space of the $\underline{K}$ vector estimated either from the simultaneous measurements of the

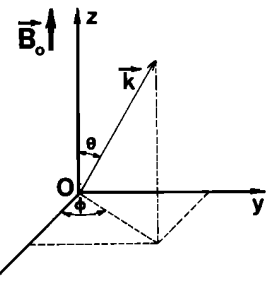

Fig. 1. Coordinate system. The Oz axis is parallel to the earth's magnetic field, Ox is in the meridian plane containing the point of observation, and Oy is oriented eastward.

[1]Now at Laboratoire en Physique et Chimie de l'Environnement, Orléans, France.

Paper number 5A0081.
0148-0227/85/005A-0081$05.00

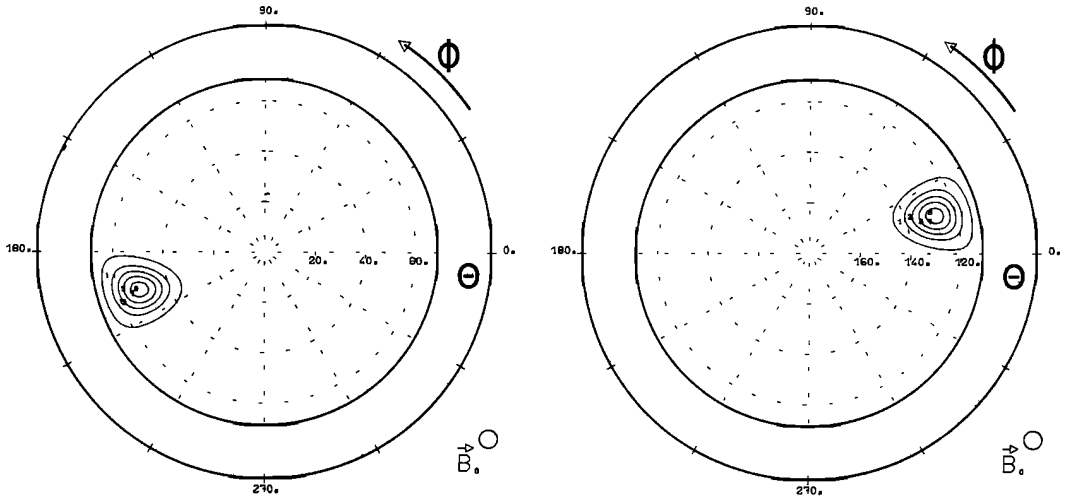

Fig. 2. Contours of the WDF of magnetic data simulated from a Dirac distribution centered at $\theta_o = 130°$, $\phi_o = 20°$. The inner circle indicates the position of the resonance angle θ_r ($\cos\theta_r = \omega/\Omega_e$). The scale of the WDF is linear and runs from 0 to 10. The units are arbitrary.

three magnetic components of the wave field (Burton and Holzer, 1974; Goldstein and Tsurutani, 1984) or from the measurement of one single component on a fast spinning satellite (Kurth et al., 1975; James, 1976). Information on the $\underline{K}$ vectors at the source ifself has even been derived from ray tracing started at the observation point from the estimated $\underline{K}$ vectors (James, 1980). In such a case, where a single $\underline{K}$ vector is considered, one must have a criterion to stop the ray tracing and to determine the source region.

As will be shown in the present paper, the problem is much easier to deal with when the observed electromagnetic field is one of a sum of elementary plane waves having different wave normal directions. Then, several ray tracings can be started with different $\underline{K}$ vectors; the convergence point, if it exists, being a possible point source. However, the use of this technique requires, first, that the $\underline{K}$ vectors be sufficiently dispersed at the point of observation, second, that their estimation be sufficiently accurate, and third that the medium between the observation and source points be correctly modeled.

2. WDF Determination

Let us consider the Cartesian coordinate system Oxyz (Figure 1) in which the Oz axis is parallel to the earth's magnetic field $\underline{B}_o$, the Ox axis is in the local magnetic meridian plane and points in the direction away from the earth, and the Oy axis is oriented eastward. In this system the $\underline{K}$ vector is characterized by the polar angle θ made by $\underline{K}$ with $\underline{B}_o$ and by the azimuthal angle ϕ, the origin of which is in the local magnetic meridian plane. The WDF is a function of these two angles and of the frequency ω. It is written $F(\omega, \cos\theta, \phi)$. Supposing that the electromagnetic field is measured at the output of narrow band filters with central frequency ω_o, it can be approximated by $F(\omega_o, \cos\theta, \phi)$ (Storey and Lefeuvre, 1980).

Let us gather the three electric wave field components e_x, e_y, e_z, and the three magnetic components h_x, h_y, h_z, in a generalized electric vector $\underline{\varepsilon}$ whose components are

$$\varepsilon_{1,2,3} = e_{x,y,z} \qquad \varepsilon_{4,5,6} = Z_o h_{x,y,z} \tag{1}$$

with Z_o the wave impedance of free space. The WDF is related to the real and imaginary part of the spectral matrix elements S_{ij} of the six wave field components ($i, j = 1 \ldots 6$) by the set of integral equations

$$P_K(\omega_o) = \iint q_K(\omega_o, \cos\theta, \phi)\ F(\omega_o, \cos\theta, \phi)\ d\sigma \tag{2}$$

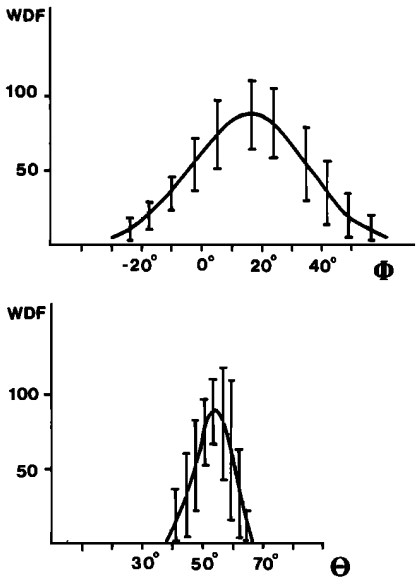

Fig. 3. Cross sections through the peak of the WDF of an Omega signal observed on board the GEOS 1 satellite. The error bars represent the variances induced on the WDF by the errors in the data.

in which $d\sigma = |\cos\theta\, d\theta\, d\phi|$ is the surface element, and the integral is taken over the surface of the sphere of unit radius (Storey and Lefeuvre, 1979). The values of P_K are such that $P_1=S_{11}$, $P_2=\mathrm{Re}[S_{12}]$, $P_3=\mathrm{Im}[S_{12}]$, ... $P_{36}=S_{66}$. The kernels $q_K(\omega,\cos\theta,\phi)$ are known analytical functions which depend implicitly on the plasma parameters, i.e., in the whistler mode, on the electron plasma and gyrofrequencies respectively denoted Π_e and Ω_e (Storey and Lefeuvre, 1980; Lefeuvre et al., 1981). The SI unit for the kernels is meters per farad, and for the WDF joules per hertz and per unit volume.

The determination of $F(\omega_o, \cos\theta, \phi)$ from the estimated values $\hat{P}_K$ of the ^oP_K is an inverse problem that admits of infinitely many solutions. We select the one which has the maximum entropy (Lefeuvre and Delannoy, 1979). Down to a normalization factor (the wave energy is not known), it is written

$$F(\omega_o,\cos\theta,\phi) = \exp\left\{-1 + \sum_{k=1}^{36} \lambda_k\, q_k\,(\omega,\cos\theta,\phi)\right\} \quad (3)$$

The Lagrangian multiplier λ_k is given values which make the quantity

$$\Phi = \frac{1}{N} \sum_{k=1}^{36} \frac{(P_k - \hat{P}_k)^2}{\langle \delta P_k^2 \rangle} \leqslant 1 \quad (4)$$

with $\langle \delta P_k^2 \rangle$ the variances in $\hat{P}_k$.

The method obviously works when fewer than six components are measured. For the measurement of three magnetic components only there are nine integral equations (2), and the subscript k runs from 1 to 9 in (4).

In fact, due to the linear dependencies between the values of q_k, one can never use the optimum number N of items of information (N = 36 for six components, 9 for three components, etc.) but a number $M \leqslant N$ of the most linearly independent. This is done in a frame of reference where the q_k are orthogonal. For more details, see Lefeuvre and Delannoy (1979).

The uncertainties in the solution are of three types: (1) nonuniqueness of the model, (2) resolving power of the model, and (3) variance errors in the model.

There is no way to avoid the type 1 uncertainties. There are infinitely many solutions to our inverse problem. Applying the maximum entropy concept consists only in selecting a smooth solution which is positive everywhere. The only guarantees we have of the validity of the method are, first, that it gives very satisfactory results in the analysis of simulated data (Lefeuvre, 1977), second, that it yields similar solutions to the ones derived by the classical methods of wave normal direction determination in the case of a quasi plane wave where the classical methods are known to be valid (Lefeuvre et al., 1982), and third, that it provides solutions which are consistent with the averaged Backus and Gilbert solution (Lefeuvre et al., 1981). Taking into account, the errors in the data in (4) increases the set of possible solutions.

The resolving power of the model (type 2 uncertainties) can be defined as a measurement of the ability of the method to describe a plane wave, i.e., to represent a Dirac distribution

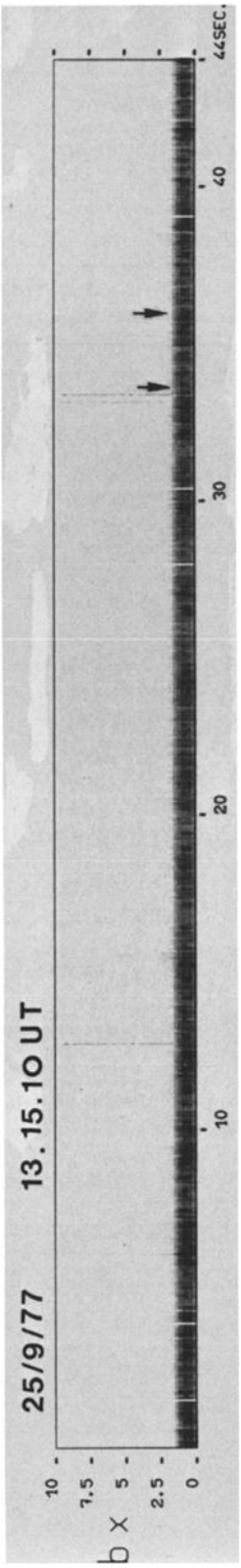

Fig. 4. B_x spectrograms of the September 25, 1977, hiss event. The satellite attitude parameters are 1315:44 UT, 1400:00 LT, L = 6.40, MLAT = 29.21°. The estimated values of the electron gyrofrequency and plasma frequency are 7.173 kHz and 29.200 kHz.

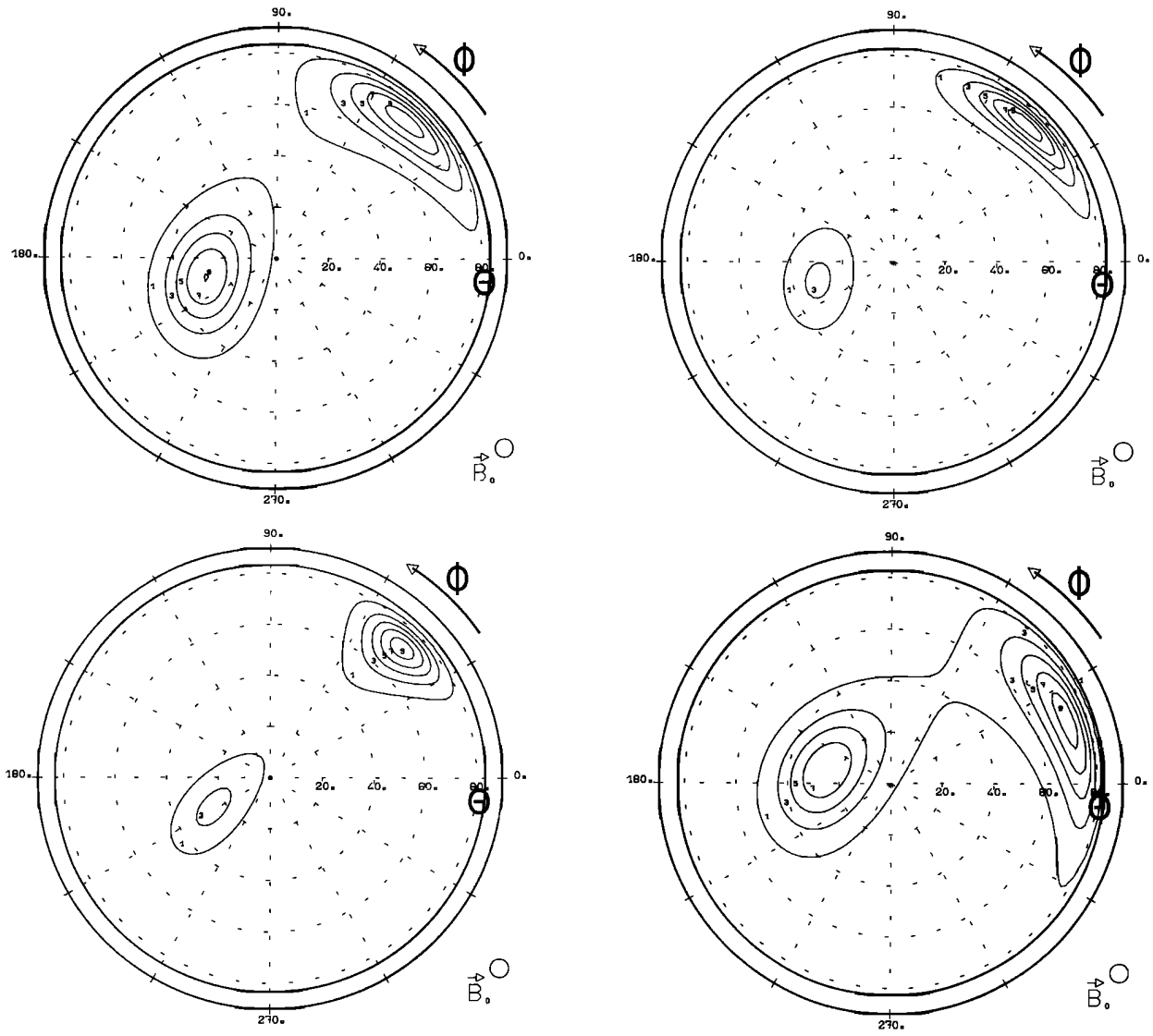

Fig. 5. WDF analysis for the september 25, 1977, hiss event. The analysis is made from the magnetic data only at two different time intervals (left and right panel) 44 s apart, and at two different frequencies (825 Hz: top panel; 923 Hz: bottom panel). We have only represented the part of the solution associated with $0 < \theta < \pi/2$.

$\delta(\omega_o, \cos\theta - \cos\theta_o, \phi - \phi_o)$. It can be numerically evaluated, by seeking the maximum entropy solution of the inverse problem where the data are the P_k calculated, for given values of the plasma parameters, while substituting $\delta(\omega_o, \cos\theta - \cos\theta_o, \phi - \phi_o)$ into (2). As an example we have presented in Figure 2 the WDF of magnetic data simulated from a Dirac distribution centered at $\theta_o = 130°$, $\phi_o = 20°$ the wave and plasma frequencies being given the values $\omega = 10$ kHz, $\Omega_e = 30$ kHz, $\Pi_e = 110$ kHz, and the numerical noise being of the order of 10% P_k. The resolution is measured by half the width of the WDF at half its maximum value. It is here of the order of 9° in θ and 12° in ϕ. Increasing artificially the noise in the data by multiplying all the variances by a factor of 5 leads to a dispersion of the order of 12° in θ and 16° in ϕ, which means that the noise has a tendency to smooth the solution.

More general ideas on the resolving power of the solution can be obtained by examining the geometrical form of the kernels (see, for instance, Figures 1 to 3 in the Storey and Lefeuvre (1980) paper). The resolving power is strong in the θ, ϕ domains where the kernels look like linearly independent while it is weak in the θ, ϕ domains where parallel slopes or zero values indicate linear dependencies. In thus considering all the kernels (electric, magnetic, and crossed), we note that the resolving power has a tendency to be poor around $\theta = 0°$ and to be good at the vicinity of the resonance angle $\theta_r (\cos\theta_r = \omega/\Omega e)$. Moreover, it increases when ω tends to be negligible relative to Ωe (this is particularly clear in Figure 1 of the Lefeuvre et al. (1981) paper). Obviously, since all the magnetic kernels have zero values at θ_r, the resolving power decreases at the vicinity of the resonance angle when magnetic data only are taken into account.

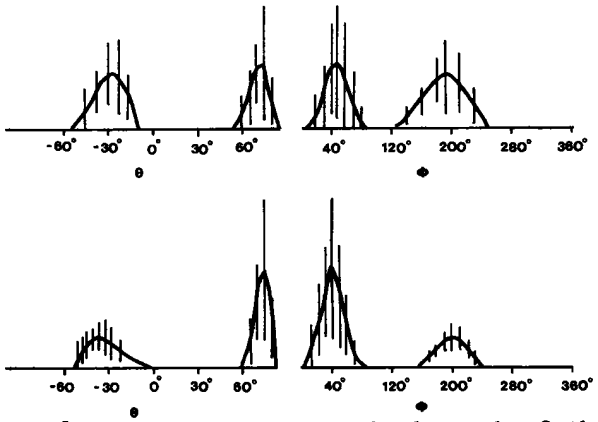

Fig. 6. Cross section through the peak of the 825-Hz WDF's of the September 25, 1977, hiss events. The errors bars measure the variances induced in the WDF by the errors in the data. In the top panel is represented the first sweep analysis, and in the bottom the second.

However, the slopes of the kernels are such that the domain actually affected is very narrow. As an example the reader will easily see from figures 1 to 3 of the Storey and Lefeuvre (1980) paper that at frequencies under half the electron gyrofrequency ($\omega/\Omega e \leqslant 0.5$) all the kernels except one (the autokernel on B_x) have their maximum values around the Gendrin (1961) θ_g angle ($\cos\theta_g = 2\,\omega/\Omega e$) for which $d(n\cos\theta)/d\theta \neq 0$. In other words the resolving power of the method is quite satisfactory even for the very large θ values we will refer to in this paper.

Errors in the data, which directly induce type 3 uncertainties, are mainly due to spectral analysis. The intrinsic magnetospheric noise and the calibration errors are supposed to be negligible. To estimate the errors in the spectral analysis, we assume that the signal is stationary in time and has a joint Gaussian distribution. Then the P_k are characterized by bias: $\langle \delta \hat{P}_k \rangle$, and autovariances and cross variances: $\langle \delta P_k \, \delta \hat{P}_l \rangle$. Under the supplementary hypothesis of a signal stationary in frequency and of errors uncorrelated between themselves, the bias and the cross variances are equal to zero. The errors in the data are then fully described by the autovariances $\langle \delta \hat{P}_k^2 \rangle$. This explains the simple form taken by the quantity (4).

The variances induced on the WDF by the errors in the data can be expressed in each point θ, ϕ by the quantity

$$\langle \delta F^2 (\omega_o, \cos\theta, \phi) \rangle = H^{-1} F^2 (\omega_o, \cos\theta, \phi) \quad (5)$$

where H is an Hessian matrix whose elements, given by $H_{kl} = \partial^2\phi/\partial\lambda_k \, \partial\lambda_l$, depend on $\langle \delta P_k^2 \rangle$ through (4). As shown in Figure 3, in the case of a man-made signal observed on board GEOS (Lefeuvre et al., 1982), it can be visualized by error bars superposed on cross sections through the peak of the WDF. Finally, the WDF is considered as stable when the parameter

$$Q = \frac{\oint\!\!\oint \langle \delta F^2 (\omega_o, \cos\theta, \phi) \rangle \, d\sigma}{\oint\!\!\oint F^2 (\omega_o, \cos\theta, \phi) \, d\sigma} \quad (6)$$

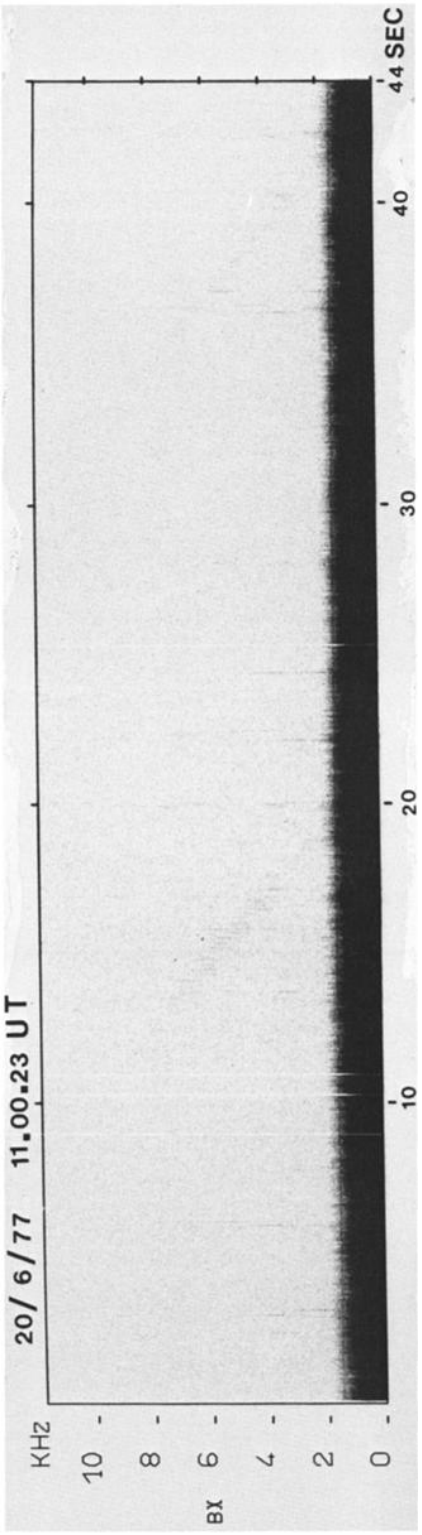

Fig. 7. B_x spectrogram of the June 20, 1977, hiss event. The satellite attitude parameters are 1700:44 UT, 1842:00 LT, L = 6.18, LAT = 19.7°. The estimated values of the electron gyrofrequency and plasma frequency are 5940 Hz and 60,180 Hz.

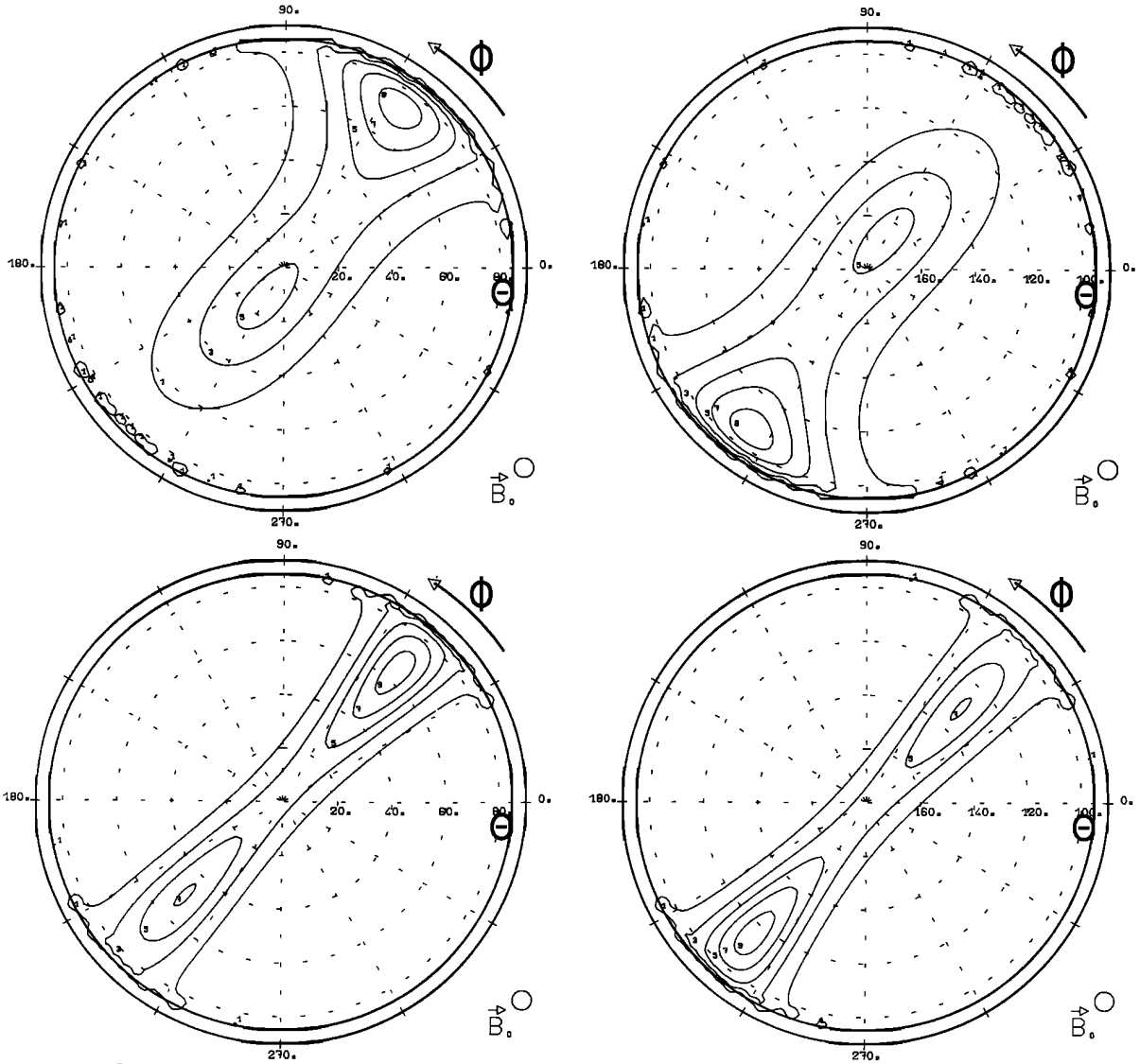

Fig. 8. WDF analysis for the June 20, 1977, hiss event. The analysis is made from the magnetic data only at two different time intervals (top and bottom panels), 44 s apart, for a wave frequency of 530 Hz. The complete solutions ($0 < \theta < \pi/2$ on the left, and $\theta > \pi/2$ on the right) have been represented.

called the stability parameter, takes a value less than or equal to 1 (Lefeuvre and Delannoy, 1979).

3. GEOS 1 WDF

S300 Experiment

In the GEOS VLF experiment (S-300 Experimenters, 1979) the three electric and the three magnetic wave field components can be measured simultaneously. Electric signals are collected by means of spheres on radial booms of length 42 m tip to tip, labeled E_y, and two pairs of spheres supported by axial booms (1.5 and 3 m long) which yield three mutually orthogonal components $e_{x,y,z}$. Magnetic signals are obtained by means of three magnetic sensors situated in a single unit on a radial boom.

The signals are subjected to several on-board analyses. Here we shall use only the analysis by the correlator and by the step frequency analyzers (SFA's). The correlator can be connected to any pair of sensors. After suitable Fourier transformation on the ground, it yields a high-resolution spectrogram in the range 0-10 kHz. The six SFA's may be connected to any sensor combination, their bandwith being only 300 Hz. In the cases we shall consider here, they are sweeping in the frequency range 0.15 - 9.6 kHz, remaining 0.69 s in each 300-Hz band, or in the frequency range 0.15 - 4.9 kHz, remaining 2.75 s in each 300-Hz band. Spectral matrices are estimated from the waveforms, on the ground, at each Fourier component ω_i.

Although many precautions have been taken in the design of the equipment and many calibration tests have been performed, at ground and on board the satellite, the measurements still suffer several limitations. First, the waveforms are not simultaneously sampled, which means that a systematic phase shift affects all the

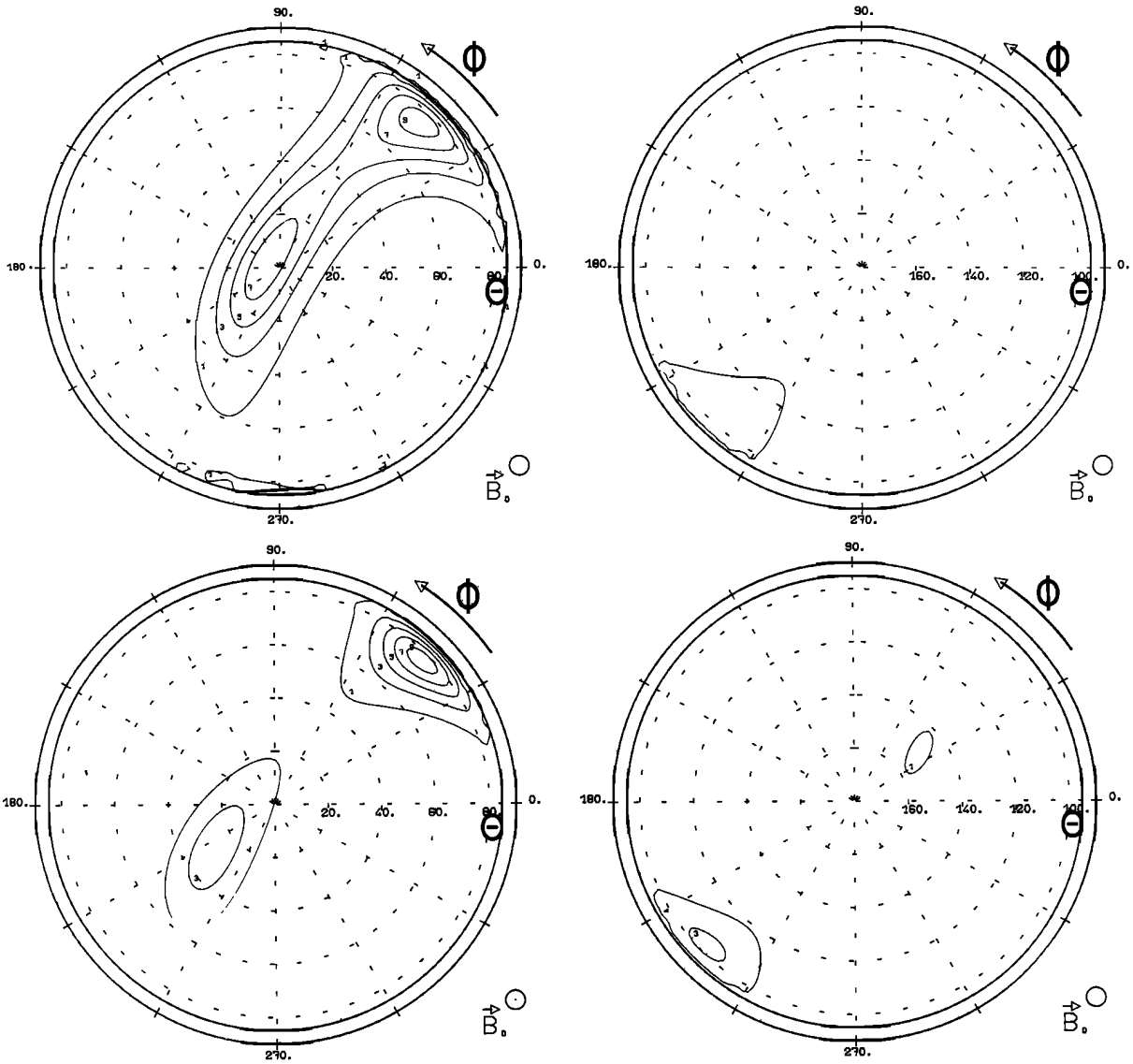

Fig. 9. WDF analysis for the June 20, 1977, hiss event from the magnetic plus the electric data. Unlike Figure 8, the solutions do not present any symmetry relative to $\theta = \pi/2$. It is clearly seen that the wave energy is converyed by waves whose longitudinal projections of the $\underline{K}$ vectors are antiparallel to $\underline{B}_o$.

cross-power spectra. A correction has been done assuming that the phase shifts were constant in each 300-Hz band. The residual error can be considered as negligible. Second, there were no on-board calibrations of the phase of the transfer function of the E_y antenna. Analysis of man-made signals (Lefeuvre et al., 1982) has shown that the phase theoretically estimated works fairly well, but there is no possibility of placing error bars. Finally, as in most similar experiments, the problem of the coupling impedance between the plasma and the spheres of the electric antenna has not been completely solved. This problem affects all the electric antennas but is still more critical for the small antennas ($e_{x,y,z}$) whose length is often smaller than the Debye length. Those two last limitations explain why the WDF analysis, which supposes the measurements of the different components are strictly related through Maxwell's equations, is generally unsuccessful when magnetic plus electric data are taken into account.

Information on the local electronic density is provided by the relaxation sounder experiment (S-301) and by the mutual impedance experiment (S-304) while the steady magnetic field is measured by the magnetometer (S-331).

Hiss Events

Up to now, 166 WDF analyses have been performed on hiss events observed on GEOS 1. A statistical study (M. Parrot, private communication, 1984) shows that 70 WDF's (42%) are found to be clearly two-peaked distributions, 37 of them (22% of the total) having a secondary peak at least half as intense as the primary peak. Among the one-peaked distributions, several are very broad, which means that they are multipeaked distributions not well resolved. Here we shall

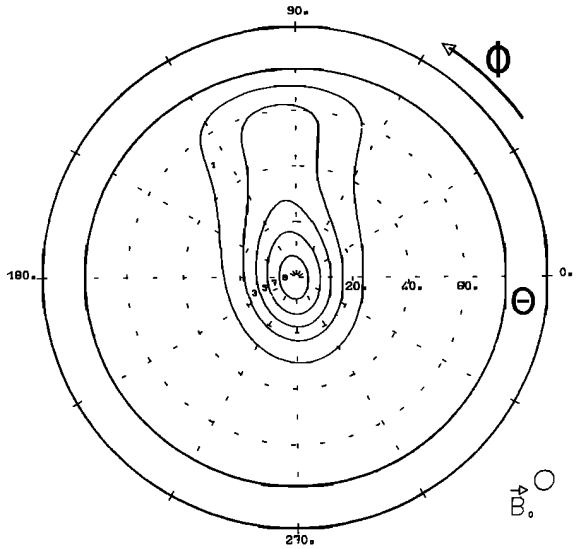

Fig. 10. Contours of the WDF obtained from the magnetic data only for a very intense chorus event observed on december 2, 1977, around 0820:45 UT and analyzed at 1.76 kHz. We have only represented the part of the solution corresponding to $\theta<\pi/2$.

focus on results of WDF analysis relative to the September 25, 1977, and June 20, 1977, hiss events. They have been chosen both because they are good examples of two-peaked distributions and because they have been observed over time intervals where the medium is easily modeled. Since the two periods are relatively quiet (Kp≤4- during the day and the two previous ones), a dipole model has been used for the field. Since the measurements take place outside the plasmasphere, far from the plasmapause, a modeling of density gradients has been avoided. Finally, S-301 and S-304 local electronic density measurements have been shown to be consistent with a diffusive equilibrium model.

A 44-s period of the b_x and E_y autopower and cross-power spectra of the September 25 hiss event, recorded at L=6.4, 1400 LT, and 29.21° magnetic latitude (MLAT), is represented in Figure 4. Since the step duration here is 2.75 s, there is only one sweep of the SFA's in the hiss band. During this sweep the more energetic signal is observed in the region indicated by the two vertical arrows. The WDF analysis has been performed on the corresponding step, at 825 Hz and 923 Hz, first from the magnetic data only, and then from the magnetic plus the electric data. However, the latter analysis, which leads to unstable solutions, will not be discussed here. Moreover, to test the stationarity in time of the results, the WDF analysis has been repeated 44 s later, at the same frequencies, during a second sweep of the SFA's in the hiss band.

Contours of the maximum entropy solutions are displayed on polar diagrams in Figure 5. The scale of F is linear and runs from 0 to 10. The outer circle corresponds to $\theta=90°$ while the inner circle indicates the position of the resonance cone for the whistler mode ($\cos\theta_r = \omega/\Omega_e$). The quantity evaluated in this analysis based on the magnetic data only is, in fact, $F[\omega_o, \cos\theta, \phi] + F[\omega_o, \cos(180°-\theta), \phi + 180°]$; however, the only quantity represented is $F[\omega_o, \cos\theta, \phi]$ with $0 \leq \theta < \pi/2$.

In order to appraise the differences between the graphs, the errors induced in the solution by the errors in the data have been estimated from (5). The results obtained at 825 Hz, for the two

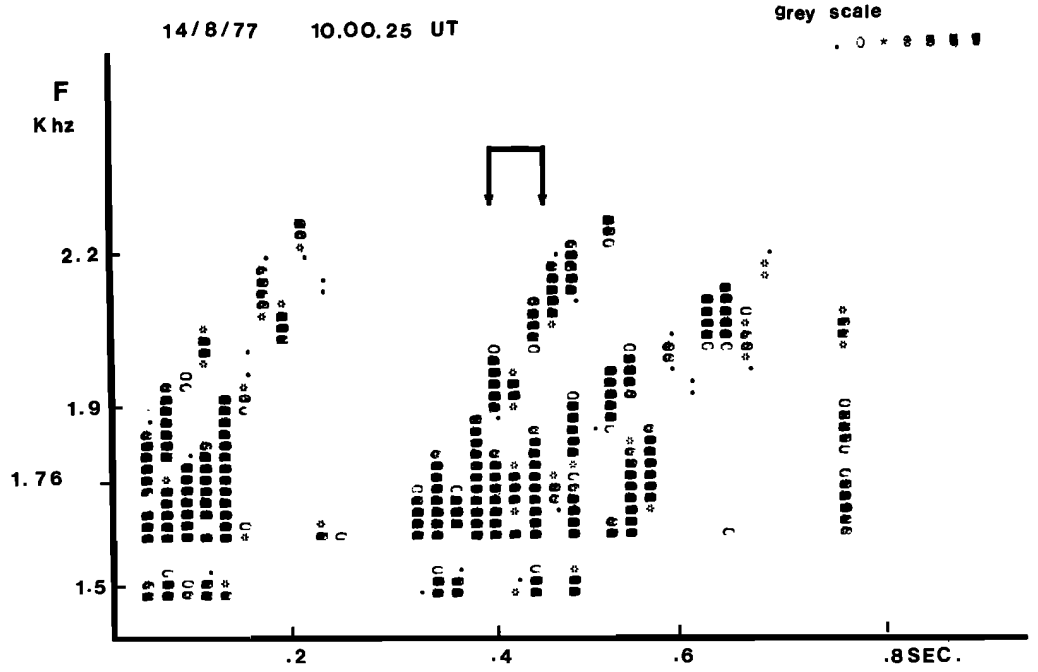

Fig. 11. High-resolution spectrum of the August 14, 1977, chorus event. Each point represents a frequency interval of 23 Hz and a time interval of 21.5 ms. The WDF analysis is made at 1.76 kHz in the time interval bordered by the two vertical arrows. The grey scale is logarithmic and has eight levels.

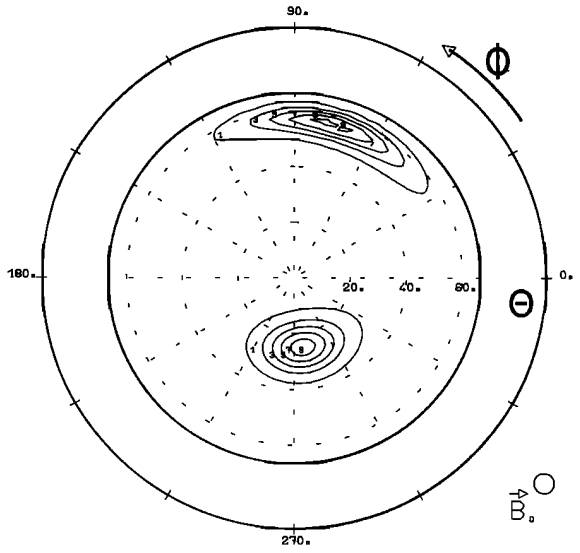

Fig. 12. Contours of the WDF obtained from the magnetic data only for the chorus element of Figure 10. We have only represented the part of the solution corresponding to $\theta<\pi/2$.

44-s samples, have been represented in Figure 6. From the figure it is clear that all the differences can be explained by known errors in the data a possible time effect being masked.

It then turns out that the hiss event on September 25, 1977, is characterized by a two-peaked WDF. The main peak is located at $\theta \simeq 70°$, $\phi \simeq 40°$. It indicates a concentration of the θ values in the neighborhood of the Gendrin angle ($\theta_g \simeq 75°$ while $\theta_r \simeq 80°$). The secondary peak, 1.1 to 4 times less intense than the main, is located at $\theta \simeq 30°, \phi \simeq 190°$. According to the uncertainties in ϕ we can consider that the two peaks are practically opposite in azimuthal angle.

A 44-s period of the b_x and E_y auto power and cross-power spectra of the June 20, 1977, hiss event, recorded at L=6.18, 1842 LT, 19.7° magnetic latitude, is represented in Figure 7. Here, the step duration is 0.69 s, which means that during those 44 s there are two sweeps of the SFA's in the hiss band.

The WDF analysis has been performed on the two sweeps, at 530 Hz, from the magnetic data only, and then from the magnetic plus the electric data. Both solutions, having been found stable, are discussed.

The solutions obtained from the magnetic data only are displayed in Figure 8 in the entire domain $0 \leq \theta < \pi$. The top panel represents the solution for the first sweep, and the bottom the solution for the second. Again two-peaked distributions nearly opposite in their ϕ values are found the main peak being around the Gendrin angle ($\theta_g \simeq 80°$), slightly off the resonance cone ($\theta_r \simeq 85°$). However, in contrast to what has been observed in the September 25 hiss event, the differences between the two solutions are too large to be explained only by errors induced in the data.

Now, probably due to better performance of the electric antennas at that particular time (see Lefeuvre et al., 1981) the WDF analysis made from the magnetic plus the electric data leads to stable solutions in the two sweeps. This enables us to answer several important questions. First, all the waves propagate with their $\underline{K}$ vectors in the earth magnetic field direction, i.e., from the equator to the north. The residual "image" of the WDF in the domain $\pi/2 < \theta < \pi$ seems to be due to the uncertainties in the electric measurements and in the plasma frequency determination. Second, although the solution is slightly modified, in the domain $0 \leq \theta < \pi/2$, from Figure 8 to Figure 9, the propagation at large θ values is confirmed. This means that propagation characteristics determined, from the magnetic antennas only, in the vicinity of the resonance angle, are reliable.

Chorus Events

Statistics on the WDF analysis of chorus events are difficult to establish at the present time. The analyses which are actually performed are based on the interpretation of spectral matrices obtained from spectral analysis methods (Fourier transforms of the correlation functions, average of Fourier transforms on the waveforms) which assume that the signal is stationary in time and is slowly varying in frequency: hypotheses which are obviously not valid. However, results obtained so far seem to indicate that chorus events with unambignous double-peaked distribution are rather the exception. This has been recently confirmed by Goldstein and Tsurutani (1984), who have used a classical method of spectral analysis, but also by D. Lagoutte and F. Lefeuvre (paper in preparation, 1985), who based their spectral analysis on

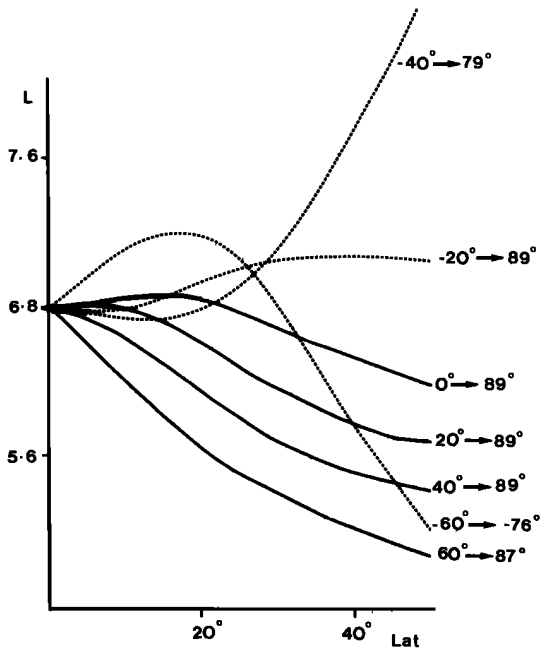

Fig. 13. Ray tracing from a source located at L = 6.8 and MLAT = 0°, and emitting in all permitted wave normal directions at a frequency ω such that $\Lambda = \omega/\Omega = 0.3$. On the right are written the starting θ values (θ_o), and on the left the θ values which would be observed at MLAT ≃45°.

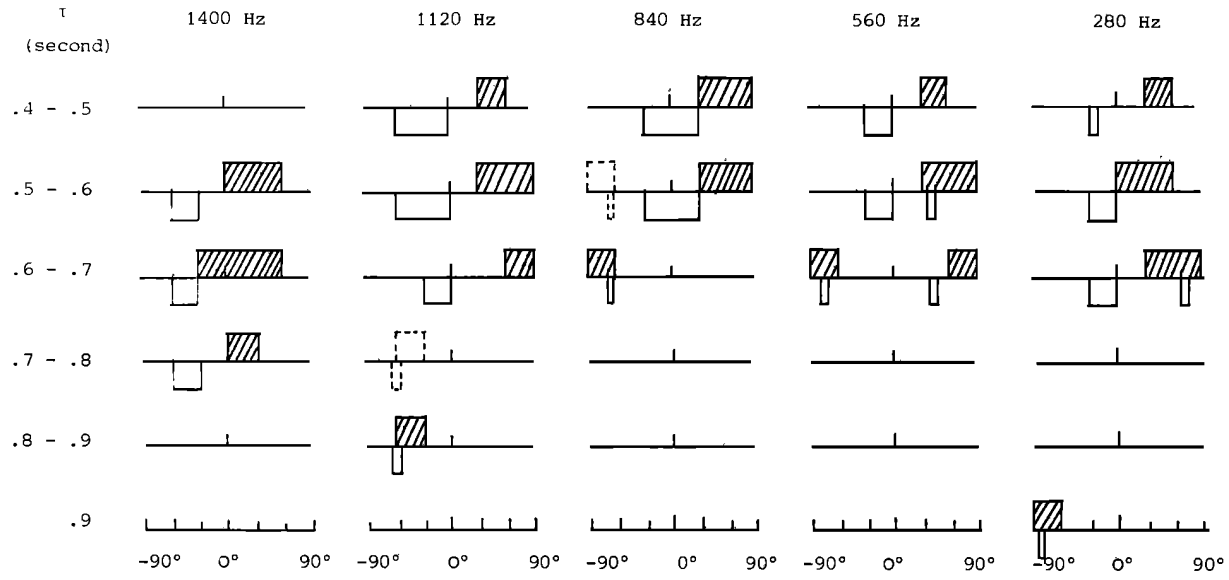

Fig. 14. Time of arrival in the region $6.9 \leqslant L \leqslant 7.1$, $20° \leqslant MLAT \leqslant 25°$, of the waves generated at L = 6.8, MLAT + 0° at five different frequencies (1400, 1120, 840, 560, and 280 Hz); the electron gyrofrequency at the source is 2800 Hz. On top of each line the hatched arrays represent the θ values represented by open arrays; under the lines, narrow arrays indicate weak dispersions in θ. Dashes represent observations just starting at the end of the time interval considered.

a vectorial autoregressive model (Lagoutte and Lefeuvre, 1983). Weak secondary peaks or broad distributions (Figure 10) might be due to errors in the spectral analysis, or to the noise produced for instance by the hiss band which usally accompanies the band-limited chorus (Cornilleau-Wehrlin et al., 1978; Koons, 1981). Now, even if they are odd, the douple-peaked chorus distribution might contain information on the source, while the others do not. That is why they are considered here.

The August 14, 1977, chorus event has been recorded at L=6.01 and at 1148 LT, in the equatorial zone (MLAT = 5.7°) for an electron gyrofrequency and plasma frequency of 4.42 kHz and 23.7 kHz respectively. A 21.5-ms resolution spectrum, obtained from the b_x SFA output, has been represented in Figure 11. We have analyzed the third element, at 1.76 KHz, in the time interval of 70 ms bordered by the vertical arrows. Contours of the solution derived from the magnetic data only are represented in Figure 12. Again, a WDF with two peaks nearly opposite in ϕ is observed. An analysis based on a two-plane wave model (Buchalet and Lefeuvre, 1981) shows that the two-plane wave model is far more likely than a single-plane wave model. Here the stronger peak has θ values greater than the Gendrin angle ($\theta_g \simeq 37°$). Although unstable, the solution obtained from the magnetic plus the electric data seems to indicate that the two wave packets are propagating with the longitudinal components of the $\underline{K}$ vectors in the $\underline{B}_o$ direction.

4. Direct Ray Tracing

Hypothesis

The two wave packets, which simultaneously reach the satellite in the cases of hiss as well as chorus, can obviously be produced by two distinct sources and be propagated to the point of observation either by a direct ray path or after several internal reflections in the magnetosphere. However, we believe that some of them at least come from the same source region for the following reasons. First, they convey a comparable amount of energy, which would be surprising for uncorrelated waves. Second, most of their $\underline{K}$ vectors are contained in the same azimuthal plane ($\phi = \phi_o$ or $\phi = \phi_o + \pi$), which is more easily attributed to a source-satellite geometry effect than to a local property of the

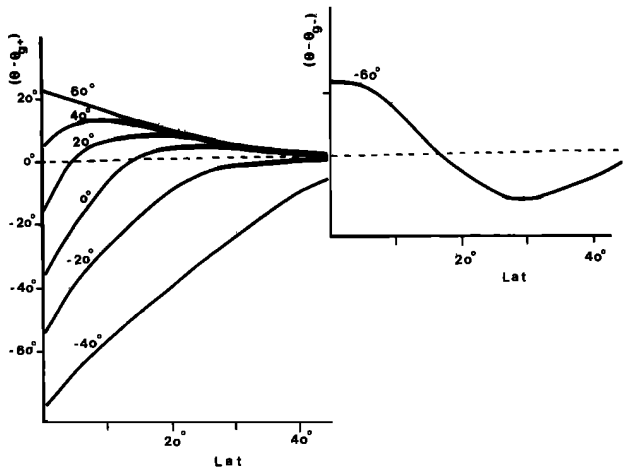

Fig. 15. Focusing of the θ values around the positive (θ_g^+) and negative (θ_g^-) Gendrin angle. The source is the same as Figure 13. The starting θ values are indicated on the right above the ($\theta - \theta_g^+$) and ($\theta - \theta_g^-$) curves.

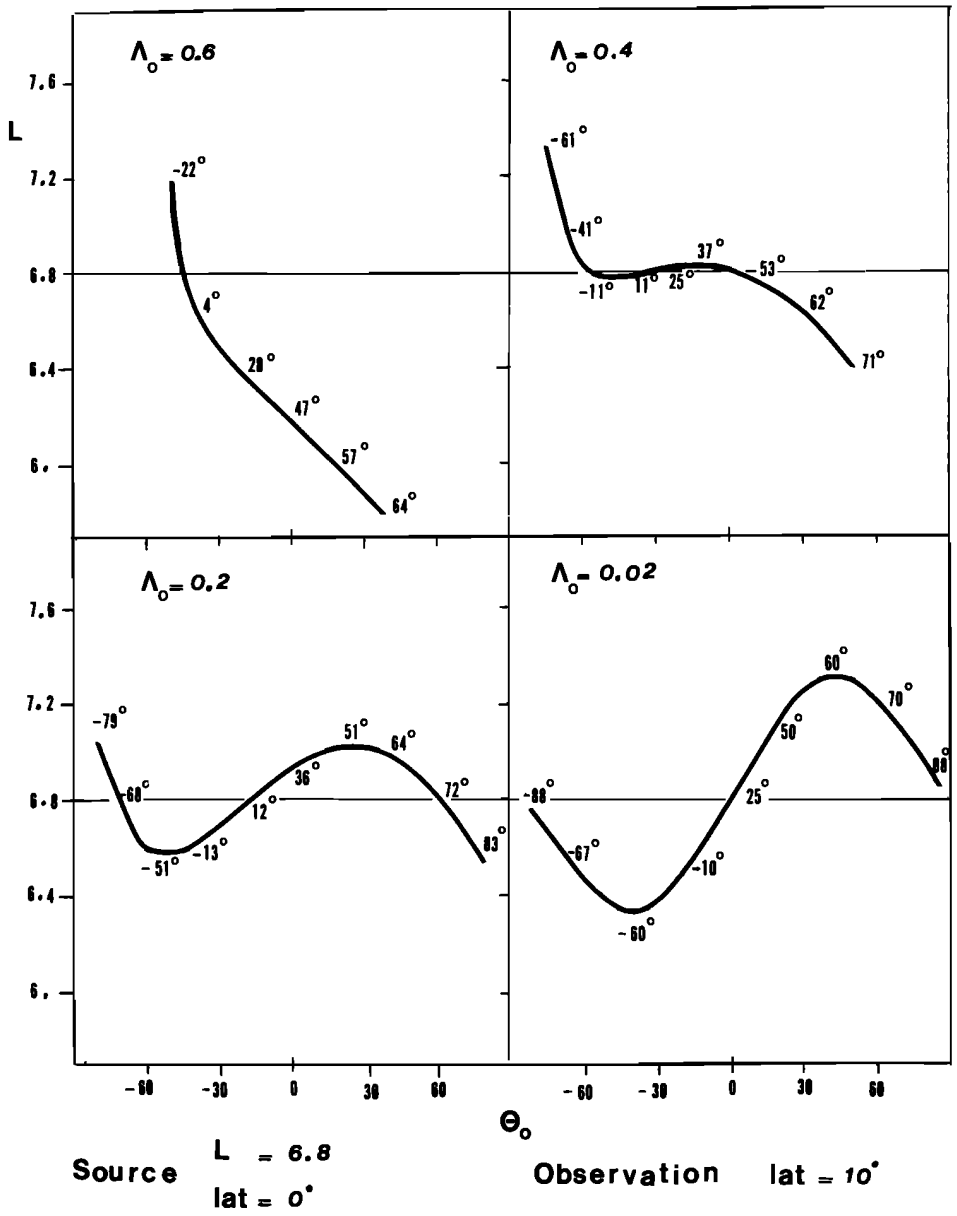

Fig. 16. Waves observed by a satellite crossing the L shells at a constant latitude value MLAT = 10°. The source is located at L = 6.8, MLAT = 0°. It is assumed to emit successively at Λ_o = 0.6, 0.4, 0.2, and 0.02. The abscissa are the θ values at the source point. The numbers written above the curves are the θ_p values at the observation point. Example for reading the graphs: a wave emitted at the normalized frequency Λ_o = 0.6 and with a θ_o angle of 30° is seen by the satellite at L ≃ 5.8; the θ value at the observation point is ≃ 62°.

medium in the generation region or at the point of observation.

We propose here to test the validity of such a model by performing direct ray tracing. We suppose a source is given and the parameters of the medium are fixed. Then we study the wave normal distribution of the waves which could reach a satellite. We stress that whereas the obtaining of a two-peaked wave normal distribution meraly establishes the fact that there is no reason to reject the model, it does not prove such a model is right. In order to simplify the calculations, several hypotheses are made concerning the source, the medium and the propagation conditions. They will be used in the direct ray tracing as well as in the inverse ray tracing (next section). Let us examine them one by one.

First, we assume that the source is isotropic, i.e., that it emits in all possible wave normal directions. This is in apparent contradiction with the idea commonly accepted that the waves are generated in a narrow cone of emission (Tsurutani et al., 1979). As a matter of fact we do not dispute this hypothesis. However, on the basis of the observations of emissions propagating at large θ angles, the equatorial region included (Lefeuvre et al., 1981, 1983), we do not see any reason to prefer a cone of emission cen-

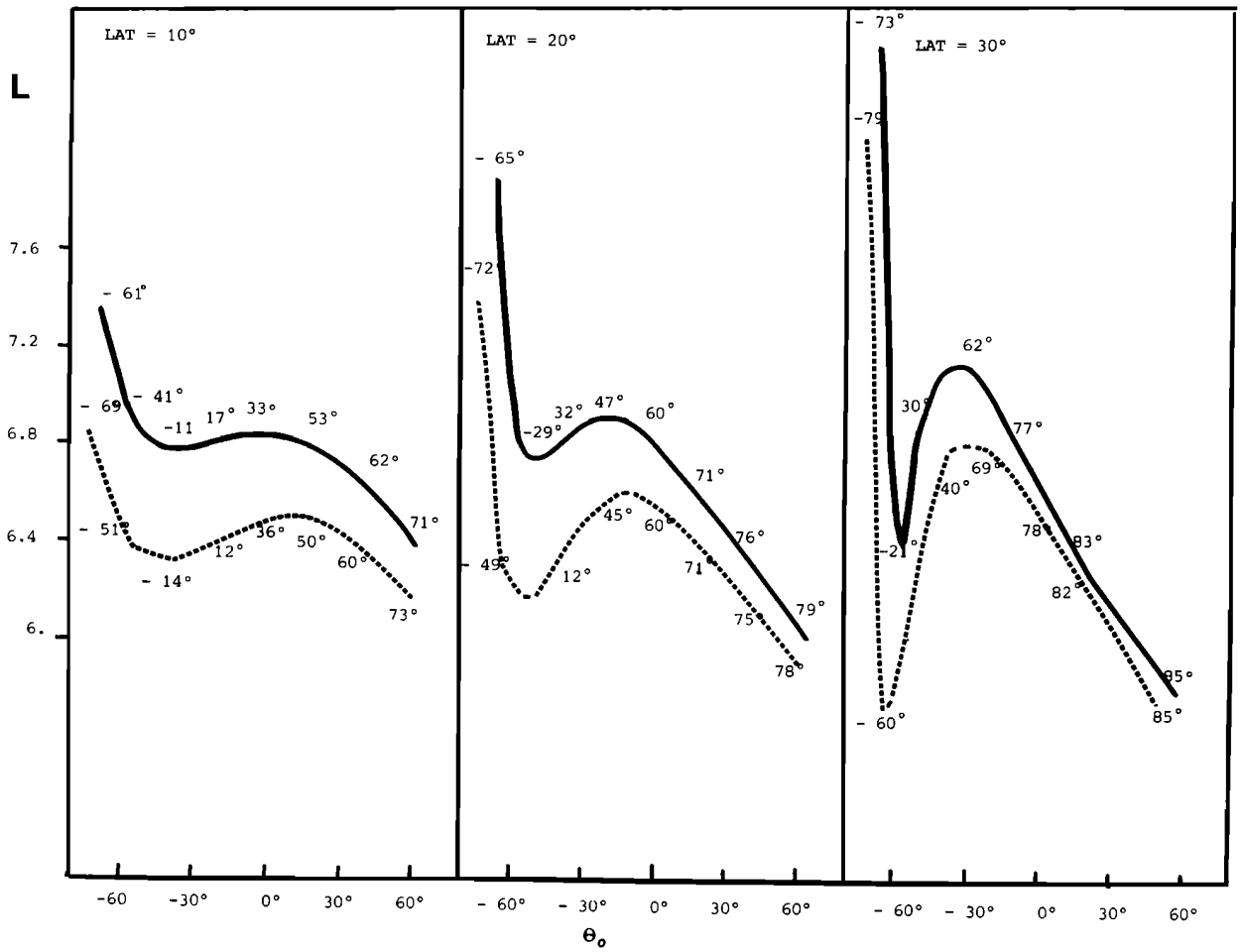

Fig. 17. Same as Figure 16. Here there are two equatorial sources, one at L = 6.8 (solid line) and the other at L = 6.4 (dashed lines). The emission is at the same frequency (1.12 kHz). The observations are made for crossings of the L shells at three different latitude values.

tered on the earth magnetic field direction, as many authors do (Burton and Holzer, 1974; Goldstein and Tsurutani, 1984). The waves at large θ values are probably not so Landau damped as is often assumed (Church and Thorne, 1983), and the instability mechanism of Kennel and Petschek (1966) and that of Etcheto et al. (1973), which favors the generation of waves at low values, are models which can eventually be adjusted. An isotropic model fits the requirement for longitudinal as well as for oblique propagation.

Second, we take a dipole field model for the earth magnetic field and a diffusive equilibrium model for the plasma. Both hypotheses have been checked via on-board measurements (S-331 for the field, and S-301 and S-304 for the plasma) for the September 25 and June 20 hiss events as well as for the August 15 chorus event.

Third, we suppose that propagation take place far from any gradient in plasma density (plasmapause) and is essentially nonducted. Such hypotheses are consistent with the observations we discuss here.

Fourth, we assume that all the $\underline{K}$ vectors are contained in the local geomagnetic meridian plane, allowing the use of the Stanford two-dimensional ray tracing program (Burtis, 1973). Such a hypothesis is difficult to justify on the basis of the propagation characteristics found for the hiss and chorus events analyzed in section 3. However, one has checked (L. Cairo, personnal communication, 1984) that the information obtained on the source position and on the distribution of the $\underline{K}$ vectors within the source is basically the same if one applies the Cerisier (1970) three-dimensional ray tracing program. Considering the simplicity of the representation and of the interpretation of the two-dimensional ray tracings, and the similarity of the findings provided by the three-dimensional ray tracing, we have chosen to refer only to the two-dimensional ray tracing. Results on the three-dimensional ray tracing, which supposes a different approach, will be published elsewhere.

Note that in the geomagnetic meridian plane the $\underline{K}$ vectors whose ϕ angles are equal to zero are oriented upward while the $\underline{K}$ vectors whose ϕ angles are equal to π are oriented toward the earth. In order to facilitate the notation, from here on we shall consider that the first ones have positive θ values ($0 \leq \theta < \pi/2$) while the others have negative θ values ($-\pi/2 < \theta < 0$). From here on the characteristic wave parameters will

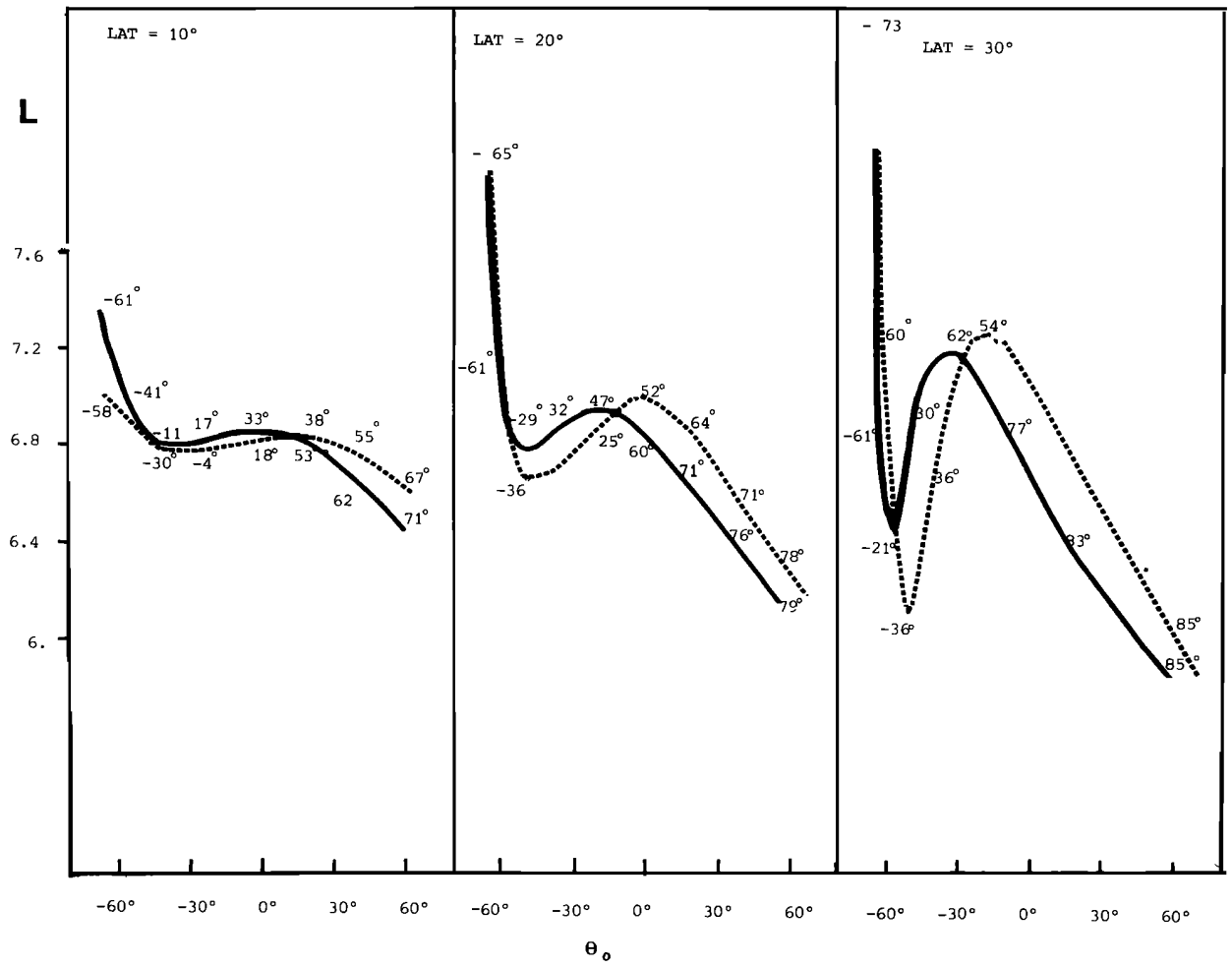

Fig. 18. Same as Figure 16. Here there are two sources at L = 6.8 ; one is at the equator, the other at MLAT = 4.6°.

be labeled with the subscript 0 when referring to the source and with the subscript p when referring to the observation point.

Ray Path From A Point Source

Let us start our simulation with a single point source located at the value L = 6.8 of the McIlwain parameter (the plasmapause is around L = 4) and at the magnetic equator (MLAT = 0°). The normalized frequency $\Lambda = \omega/\Omega_e$ at the equator is given the value $\Lambda_o = 0.3$, which is less than the limit $\Lambda = 0.5$ where the propagation laws change. Rays corresponding to plane waves emitted with different θ_o values are traced on an L versus MLAT graph (Figure 13). For waves emitted with negative θ_o values the ray paths are shown with dashed lines while the others are shown with solid lines. On the right are written the θ_o values at the equator (θ_o) and then the θ_o values at MLAT ≃ 45°. As already pointed out by Burtis (1974), it is clear that waves emitted with different θ_o values can reach the same point of observation after having followed different ray paths.

This point is made still clearer in the following simulation. Rays are generated from the same source point (L = 6.8, MLAT = 0°), at 1400, 1120, 840, 560, and 280 Hz (Λ_o = 0.5, 0.4, 0.3, 0.2, and 0.1), with polar angles θ_o spaced by $\Delta\theta_o$ = 5°. A rough statistic is made on the arrival time τ and on the θ_o values θ_p of the waves which reach the region: $6.9 \leqslant L \leqslant 7.1$, $20° \leqslant$ MLAT $\leqslant 25°$. The results are summarized in Figure 14. At 1400 Hz all the rays arrive between τ = 0.5 and 0.8 s. The θ_p values are generally positive (or if negative, close to 0°). They have been emitted with θ_o values such that $-60° \leqslant \theta_o \leqslant -30°$. At 1120 Hz the situation is slightly more complex. Positive θ_p values are observed at $0.4 \leqslant \tau < 0.6$, while large negative θ_p values are seen at $0.8 \leqslant \tau \leqslant 0.9$ s. The first have been generated from a wide angular spectrum ($-60° \leqslant \theta_o \leqslant 0°$, or $-30° \leqslant \theta_o \leqslant 0°$), and the second with a narrow angular spectrum centered on $\theta_o = -60°$. Although some negative θ_p values (dashed arrays) may be seen at $\tau < 0.8$ s, it seems difficult to observe the two-peaked WDF's, described in the previous section, for a nonstationary phenomenon of the chorus type. However, this is quite possible, particularly for fuzzy chorus elements, at 840 Hz and above all at 560 Hz. In the first case the negative θ_p values are due to waves generated at $\theta_o \simeq -65°$ while the positive θ_p values are produced by a wide angular spectrum centered on $\theta_o = 0°$. In the second, the two wave packets are

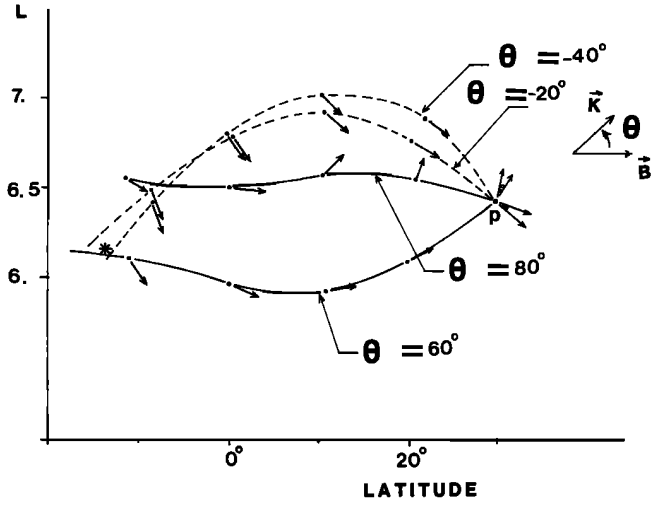

Fig. 19. Inverse ray tracing from the observation point for the September 25, 1977, event. The asterisk only represents the crossing point of the rays that started with θ_p values equal to the θ_p values of the peaks of the WDF's.

generated by very narrow angular spectra, one at $\theta_o = -75°$, the other at $\theta_o \simeq 40°$. At 280 Hz there is nearly 1 s between the arrival times of the positive and negative θ_p angles, which means that a two-peaked WDF can be found only for phenomena very stationary in time.

Note that the situation is about the same if the observation is made on a satellite which moves in relation to the point source. At 280 Hz, with a satellite velocity of the order of 5 km/s, the Doppler effect does not exceed 2 Hz, even for waves propagating at very oblique θ angles ($\tau < 0.95$). At the other frequencies where the waves are not so oblique, it is less than 0.5 Hz.

Confirming the observations made from the GEOS data, we also find that, moving away from the source, the values of the simulateds waves concentrate around the Gendrin angle, reaching the resonance angle when both angles are practically merged, i.e., when the local normalized frequency is such that $\Lambda << 1$. This is illustrated in Figure 15 where the differences $\theta - \theta_g^+$ (with θ_g^+ the positive Gendrin angle) and $\theta - \theta_g^-$ (with θ_g^- the negative Gendrin angle) are plotted versus the magnetic latitude MLAT; the θ values at the emissions are written above the curves. One check is that 20° off the equator most of the waves have θ values that are within 10° of the Gendrin angle. All the θ values have converged toward θ_g for MLAT = 40°, when $\theta_g \simeq \theta_r$. The rapidity of the convergence toward θ_g is a function of the Λ values. As a matter of fact it decreases with Λ.

Now even if the model of an isotropic point source seems to be perfectly consistent with the two-peaked WDF's of Figures 5, 8, and 9 and if it can eventually be used for the WDF of Figure 12, it does not explain all the observations made on the GEOS satellite. This is the case of a two-peaked WDF found for a chorus event on September 21 around 0700 UT. The event is observed practically up to 4 kHz. The plasma parameters are $\Omega_e = 6$ kHz and $\Pi_e = 20$ kHz. The analysis is made at $\omega = 3.33$ kHz, i.e., for a local value of Λ greater than 0.5 ($\Lambda = 0.55$). The simultaneous presence of two wave packets implies either that the source is extended in L and MLAT values or that the waves which are observed come from different region sources. In the present case where the power spectra seem to indicate a mix of different chorus elements, it is the latter hypothesis which is the most likely.

Observation on a Satellite

To have a better understanding of the GEOS 1 observations, let us examine whan can be received on a satellite crossing the L shells of the earth magnetic field at constant magnetic latitude values when the source, assumed to be localized and isotropic, is located at the equator (MLAT = 0) at L = 6.8. To illustrate, we plot the L values at which a wave emitted with a given θ_o angle (the abscissa) reaches the latitude of observation; some θ_p values at the point of observation are given for information (Figures 16 to 18). The energy transfer from the source to the satellite is measured by the ratio $\Delta L/\Delta\theta_o$. It is optimum for $\Delta L/\Delta\theta_o \longrightarrow 0$ and minimum for $\Delta L/\Delta\theta_o \longrightarrow \infty$.

The results at MLAT = 10°, for waves emitted at $\Lambda_o = 0.6$, 0.4, 0.2, and 0.02, are summarized in Figure 16. As predicted, for $\Lambda_o > 0.5$, only a single wave can be detected at each L value since the energy transfer is far from optimum. For $\Lambda < 0.5$ there is a zone, centered on the L value of the source, for which several waves can be simultaneously observed. Hence for $\Lambda_o = 0.4$ the waves emitted at $\theta_o \simeq -60°$, as well as the waves emitted at - 25° and 0°, are seen at L = 6.8 with θ_p values at the point of observation respectively of the order of - 20°, + 25°, and + 40°. The zone of multiple observations increases when Λ_o is decreased while the efficiency of the energy transfer decreases. The zone disappears for very low Λ_o values (see $\Lambda_o = 0.02$) where the more oblique waves fall in the resonance cone before reaching the satellite position. The optimum zone of multiple observations is not easy to determine. It could relate to the $\Lambda = 0.34$ peak in chorus occurrence observed on OGO 3 (Burtis and Helliwell, 1976).

As shown in Figure 17, following, for instance, the solid curves, the zone of multiple observations at 1.12 kHz extends in L values when the satellite crosses the L shells at higher latitudes. This is consistent with statistics made on the WDF's of the GEOS 1 hiss event (M. Parrot, personal communication, 1984).

In the same figure have been superposed the L versus θ_o graphs representing the observation on the same satellite of a second point source located also at the equator, but at a lower L value (L = 6.4), and emitting at the same frequency (1.12 kHz). Although most waves of the two sources are seen at different L values for a point of observation close to the source (MLAT < 20°), they tend to merge at greater distances. Assuming a continuous source between L = 6.4 and 6.8, one can observe several wave packets. Hence at MLAT = 30° and L ≃ 6.6 we see, reading from left to right, first a wave packet where the θ_p values vary between - 40° and - 70°, a second whose θ_p values vary between 0° and 40°, and a third where the θ_p values are concentrated

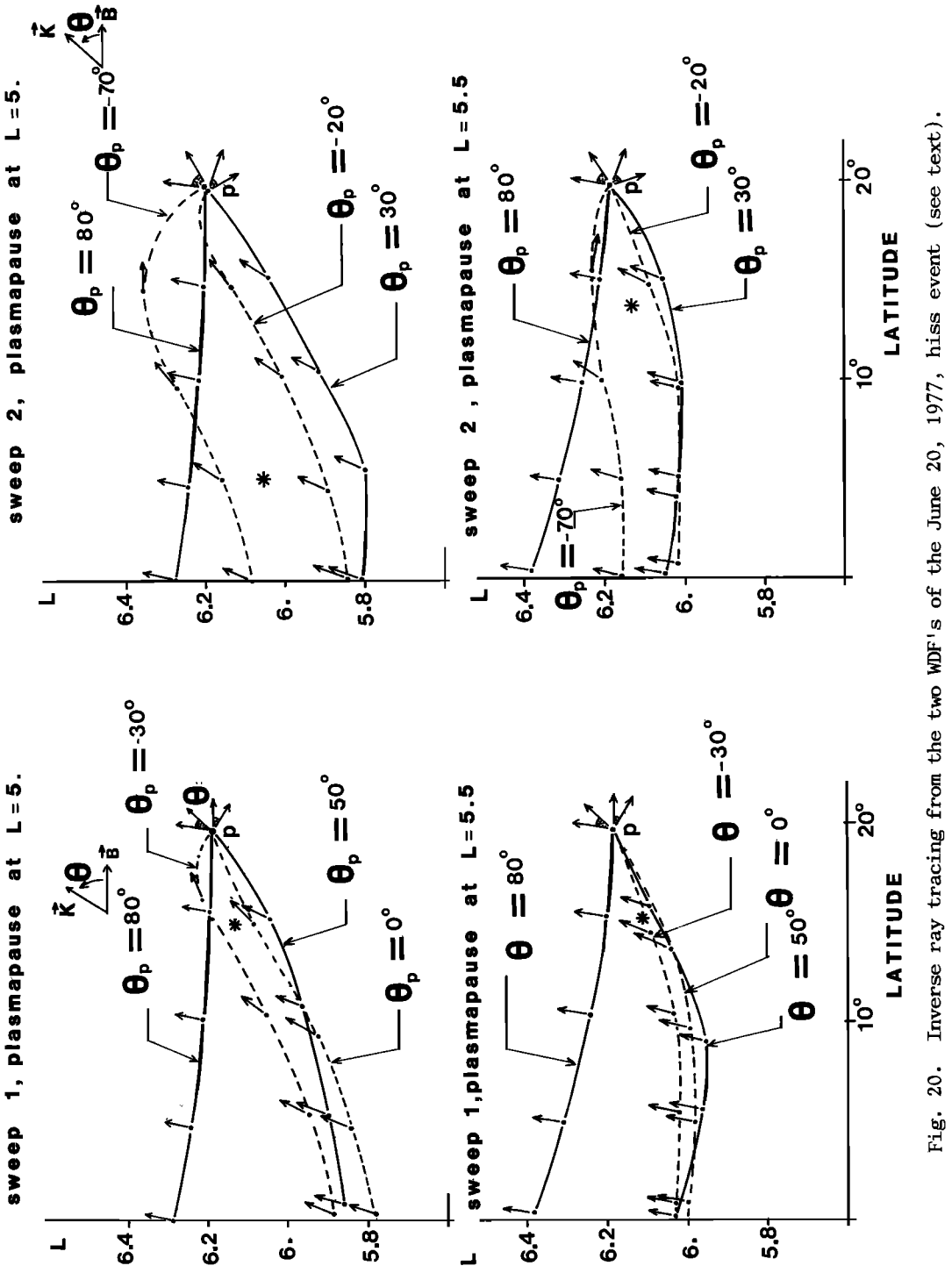

Fig. 20. Inverse ray tracing from the two WDF's of the June 20, 1977, hiss event (see text).

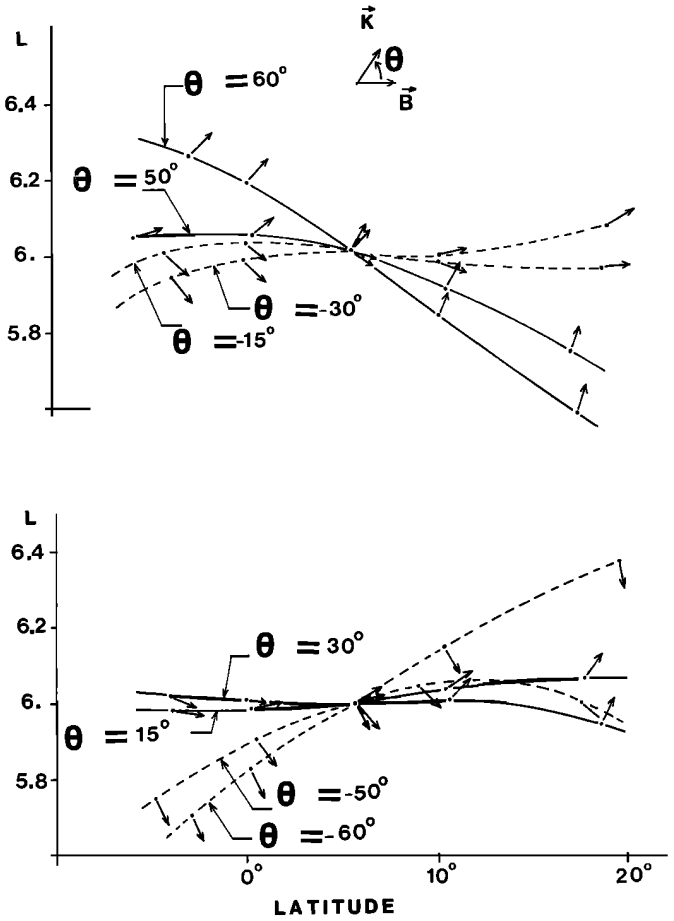

Fig. 21. Inverse ray tracing from the WDF of the August 14, 1977, chorus event. Top panel: the small θ values (θ_p = 15°, 30°) are given the azimuthal value $\phi_p = \pi$ (curves 2,1) and the large θ values (θ_p = 50°, 60°) are given the azimuthal value $\phi_p = 0$ (curves 4,3). Bottom panel: the values of the azimuthal angles are reversed.

around 78°. The weak energy transfer between the point source and the satellite ($\Delta L/\Delta\theta_o \longrightarrow \infty$) is compensated for by the extension of the source region between L = 6.4 and L = 6.8. In the same way, extending the source in latitude (Figure 18), one broadens the observed wave packets, some of them having a tendency to overlap.

Note that to a certain extent, which has still to be defined, extended sources might explain some two-peaked WDF's observed for local Λ values greater than 0.5.

The fact that three-peaked distributions suggested by Figures 17 and 18 are not observed in GEOS 1 data may have several explanations. First, due to the poor resolution of the WDF's in the θ, φ domain, two close peaks might be seen as a single broad peak. Such an explanation seems to work well, particularly with the broad WDF of the June 20 hiss event. Second, the source might be nonisotropic, which would mean, for instance, that the peaks due to the rays that started with small θ values do not exist. We shall see now that this is effectively what comes out from the inverse ray tracings.

5. Inverse Ray Tracing

Inverse Problem

In a given medium the ray tracing programs are perfectly invertible. The ray path traced from the point of observation to the source, with an initial $\underline{K}$ vector $\underline{K}_p$ and a final $\underline{K}$ vector $\underline{K}_o$, is exactly the same as the ray path traced from the source to the point of observation with an initial $\underline{K}$ vector $-\underline{K}_o$ (here the minus sign means a change of $\pi - \theta_o$ in θ and of π in φ), the final $\underline{K}$ vector being obviously $-\underline{K}_p$. Therefore, assuming the characteristic parameters of the medium are known, we can consider that the problem of localizing a source from a WDF estimated in a fixed point of space is an inverse problem which is well posed, i.e., which admits a unique solution.

However, the accuracy of the localisation is a function of the source satellite geometry and of the plasma composition. Close to the generation region, and in a low-density plasma, a good resolution can be expected, at least if the WDF is accurate enough. On the other hand, far from the generation region, and in a dense plasma, the localisation of rays coming from different sources is such that there are strong uncertainties in Figures 17 and 18.

The wave normal distribution at the source can be stable even if there are strong uncertainties in the exact source positions. At MLAT = 30°, for instance, whatever the exact L and MLAT values of the source in the domain $6.4 \leqslant L \leqslant 6.8$, $0° \leqslant MLAT \leqslant 6°$, we are sure that a wave observed with $\theta_p \simeq 80°$ has been emitted with $\theta_o \simeq 20°$.

The hypotheses made for inverse ray tracings are the same as in section 4, except that we no longer need to assume an isotropic source. As already stated, the debatable hypothesis we make here is that the waves propagate in the magnetic meridian plane. The variation of the θ values along the ray path depends on the initial value of the azimuthal angle made by the $\underline{K}$ vector (Thorne, 1969). Taking $\phi_p = 0$ at the very point of observation where the WDF indicates values of the order of 60° or 70° induces errors in the source position as well as in the wave normal distribution determination at the source. We can expect those errors not to be too important when the source-satellite distance is not too large. This has been checked by applying the Cerisier (1970) three-dimensional ray tracing program (Cairo, personal communication, 1984). Detailed results will be published elsewhere.

September 25, 1977, Hiss Event

As a first approximation we can consider that the wave energy of the September 25, 1977, event is conveyed by two wave packets, one having its $\underline{K}_p$ vectors with θ_p values included within the interval 60°, 80° and the other its $\underline{K}_p$ vector with θ_p values included within the interval [- 40°, -20°]. The shift in θ_p between the solutions of Figure 5 has no importance here since the rays are traced assuming that all the $\underline{K}$ vectors are contained in the local magnetic meridian plane (φ=o or π).

Rays traced from the observation point P (L = 6.43, MLAT = 29.1°) with θ_p values equal, on

the one hand to 60° and 80° and on the other hand to - 40° and 20°, are displayed in Figure 19. Although the ray tracing does not garantee convex properties between the rays, particularly in the vicinity of the starting point, most of the rays started with θ_p values between 60° and 80° or between - 40° and - 20° stay in the limit of the curves plotted in Figure 19. This is the case, for instance, of the rays starting with θ_p values equal to the θ values of the peaks of the WDF, and for which the crossing point has been represented by an asterisk.

Let us first try to interpret separately the ray tracings that started with negative θ_p values (dashed lines) and with positive θ_p values (solid lines). Rays represented as dashed lines crossed at a point whose coordinates (here $L \simeq 6.7$, MLAT $\simeq$ - 30°) are very sensitive to slight variations in the medium parameters. The wave normals are very oblique ($\theta < - 60°$) over the major pat of the ray path, the equatorial region and the region around the crossing point included. This demonstrates that the Landau damping is not very efficient or is negligible in relation to the amplification rate. Rays represented as solid lines do not cross. According to the concentration in azimuthal angle of the $\underline{K}$ vectors observed at point P ($\phi \simeq 45°$) this probably means that the source (or amplification) region occupies a broad region of space ($6 \lesssim L \lesssim 6.5$, $- 20° \lesssim$ MLAT $\lesssim 0°$). Again, most of the $\underline{K}$ vectors have large negative θ values.

It then turns out that the waves observed at point P, with positive as well as negative θ values, emerge from the same, very broad source region ($6 \lesssim L \lesssim 6.5$, $- 20° \lesssim$ MLAT $\lesssim 0°$). The wave normals within the source are concentrated in a very narrow cone of propagation, $-85° \lesssim \theta \lesssim - 55°$. Referring to figure 17and 18, we note that the absence of an emission cone at positive θ values seems to contradict the hypothesis of an isotropic source (section 4).

June 20, 1977, Hiss Event

Because of real modifications of the hiss event in the time interval of 22 s, or of uncertainties in the course of the analysis, the differences between the WDF's of Figures 8 and 9 are much too important to allow a unique ray tracing study as in the previous case. Accordingly, we have considered θ_p intervals of [50°, 80°] and [- 30°, 0°] for the WDF of the first sweep (top panel of Figure 8) and θ_p intervals of [30°,78°] and [- 70°, - 20°] for the WDF of the second sweep (bottom panel of Figure 8). Moreover, as plasma measurements made on board GEOS have shown that we were relatively close to the plasmapause, which is not surprising at 1842 LT under magnetically quiet conditions, each study has been done under two hypotheses. In the first the inner bound of the plasmapause has been fixed at L = 5 while in the second it has been fixed at L = 5.5. The results of the four analyses are displayed in Figure 20 with the same conventions as Figure 19.

In the light of the previous remarks, several comments can be made.

1. As already stated, the asterisk showing the crossing point between the rays that started with θ_p values equal to the θ values of the peaks of the WDF's, does not represent a point source. However, it is very useful for evaluating the displacement of the region source, from one sweep of the SFA's to the other, or from one plasmapause position to the other.

2. Rays seem to emerge from a common region as broad as the observation point is far from the plasmapause.

3. In contrast to what was observed in the September 25 hiss event, the source is probably on the same side of the equator as the observation point.

4. Except in the close vicinity of the observation point, the wave normals have large positive θ values ($45° \leqslant \theta \leqslant 80°$), which means that the remarks already made about the efficiency of the Landau damping or on the amplification mechanisms still hold. The reader will note that on September 25 the $\underline{K}$ vectors had large negative θ values within the source.

5. In Figures 10 and 18, the absence of a cone of emission at negative θ values is an indication that the source is not isotropic.

August 14, 1977, Chorus Event

Because the two peaks of the WDF of the August 14, 1977, chorus event (Figure 11) are practically 90° off the magnetic meridian plane, two calculations have been done. In the first, the peak corresponding to the large θ values ($50° \leqslant \theta_p \leqslant 60°$) has been given the azimuthal value $\phi = 0°$, and the peak corresponding to the small θ values ($15° \leqslant \theta_p \leqslant 30°$) has been given the azimuthal value $\phi = \pi$. In the second the azimuthal values are reversed. In both cases, rays have been traced toward and away from the equator (Figure 21).

In the present ray tracings, as well as in the three-dimensional ray tracings (L. Cairo, personal communication, 1984), no clear common source region can be found. This can be interpreted in several ways. First, the spectral matrix estimation, performed with a method inadequate for signals of the chorus type, leads to an erroneous WDF. In such a case, ray tracings have no meaning. Second, the observation is made within the source region. However, such a hypothesis does not fit with the slope of the risers of Figure 11, which rather indicates that the chorus elements have been propagated. Third, at the observation point, there is a merging of waves generated in different regions of space. This is actually the more probable explanation.

6. Conclusion

Wave distribution functions (WDF) obtained for natural electromagnetic emissions observed on GEOS 1 have been interpreted in two different ways. First, a model source has been assumed, and the propagation characteristics of the waves have been evaluated, at different points of space, by direct ray tracings. Second, region sources have been located, and the wave normal distribution in the sources estimated, by inverse two-dimensional ray tracings started from estimated WDF's.

Direct ray tracings have enabled us to demonstrate that waves, generated from a single isotropic point source, can reach a point of space by different ray paths, producing multipeaked WDF's.

According to the errors in the data and to the limitation in the resolving power of the method, those multipeaked WDF's may easily be seen as two- peaked distributions similar to the one determined for the GEOS data. Even, if such a model seems to be well adapted for phenomena of the hiss type, for which the stationarity in time masks the differences in time delay of the different waves, it probably does not work for phenomena of the chorus type, known as very weakly stationary in time. It has been noted that the probability of obtaining a two-peaked WDF is maximum when the observation point is at the L value of the source. It increases when the normalized frequency at the source (Λ_o) is decreased and/or when the source-satellite distance is increased. Furthermore, direct ray tracings have taught us that there is a tendency, for the unducted waves, to be propagated with their θ values close to the Gendrin angle which approaches the resonance angle as Λ tends toward zero.

Inverse ray tracings, started from the propagation characteristics determined by the WDF's, and performed for field and plasma parameters measured on GEOS, have enabled us to obtain information on the recent history of the observed waves. For VLF hiss it is shown that waves characterized by a two-peaked WDF emerge from the same broad region of space, located near the equator, and extended in L value ($\Delta L \simeq 0.5$) as well as in MLAT value (ΔMLAT $\simeq 10°$ or more). In this region the wave normals are very oblique, which demonstrates that the Landau damping effect is small relative to the amplification rate. Those findings seem to be typical of VLF hiss observed out of the plasmasphere. The question of whether such regions can be identified as source regions or not is very delicate. However, it is a hypothesis which cannot be ruled out. Inverse ray tracings performed from a single chorus element do not allow us to draw a clear conclusion. They seem to indicate that the two-peaked WDF determined is caused by waves coming from different point sources. In any case a two-peaked WDF observation is rather the exception for chorus, which is consistent with direct ray tracings.

Note that three-dimensional ray tracings performed on the emissions discussed here confirmed the two-dimensional ray tracings (L. Cairo, personal communication, 1984).

Now, if the regions of space from which the September 25, 1977, and the June 20, 1977, hiss events emerge are effectively source regions, what can be said about generation mechanisms? Most of the present thinking on the subject is based on the quasi-linear theory introduced by Kennel and Petschek (1966) and evaluated in more detail by Etcheto et al. (1973). In this theory the waves are amplified, in the equatorial regions, by the Dopppler-shifted electron gyroresonance instability. The main problems are, first, that important growth rates are obtained for propagation vectors parallel to the earth magnetic field direction only (Kennel and Thorne, 1967) and, second, that even for such waves, growth rates theoretically predicted for a pass of the wave through the amplification region are not sufficient to account for hiss intensities observed experimentally. One cculd expect to modify the condition for obtaining a maximum growth rate by varying the particle distributions used in the calculation. Operating that way, Brinca (1972) predicts large growth rates for oblique propagations, but for frequencies close to half the electrongyrofrequency only. Another way to adjust the Kennel and Petschek mechanism to the data would be to compensate the weakness of the wave amplification by recycling a large amount of the energy back to the equator. Such a model has been proved to work very well (Roux et al., 1982; Rauch and Roux, 1982) for waves observed on GEOS 1 and 2, below the protongyrofrequency. Waves emitted in the left-handed mode are returned in the equatorial region following very closed paths. The focusing of the rays compensates the obliqueness of the $\underline{K}$ vectors in the amplification region. However, the first three-dimensional ray tracings show that the process is not so efficient in the ELF and VLF ranges. As a consequence one must probably look for another generation mechanism. Although it is beyond the scope of this paper to propose new theories, it seems that a first step of research would consist in trying to reconciliate the Kennel and Petschek mechanism with the data by taking into account feedbacks of the wave field on the particle distribution function in a manner similar to that of Helliwell and Inan (1982) for the generation of discrete emissions and chorus.

The problem is very different for plasmaspheric hiss, for which reflections at the plasmapause allow the waves to return, with $\underline{K}$ vectors along the earth magnetic field, in the equatorial region (Church and Thorne, 1983; Huang et al., 1983). However, if a new generation mechanism is found outside the plasmasphere, it will be surprising if it does not apply inside.

Acknowlegments. The authors wish to express their sincere thanks to L.R.O. Storey, T. Bell, D. Carpenter, and U. S. Inan for helpful discussions and comments. They also thank T. Miller and L. Cairo for assistance in the application of ray tracing techniques and M. Parrot, from LPCE, Orleans, France, for his participation in the wave distribution function analysis of the GEOS 1 data. F. Lefeuvre's research was supported by a National Science Foundation U.S./Centre National de Recherche Scientifique France Exchange Award.

The Editor thanks B. Tsurutani and H.G. James for their assistance in evaluating this paper.

References

Brinca, A.L., On the stability of obliquely propagating whistlers, J. Geophys. Res., 77, 3495, 1972.

Buchalet, L. J., and F. Lefeuvre, One and two-direction models for VLF electromagnetic waves observed onboard GEOS 1, J. Geophys. Res, 86, 2377, 1981.

Burtis, J. W., User's guide to the Stanford VLF raytracing program, Internal report, Radiosci. Lab., Stanford Electron. Lab., Stanford Univ., Stanford, Calif., 1973.

Burtis, J. W., Magnetospheric chorus, Tech. Rep. 3469-3, Radiosci. Lab., Stanford Electron. Lab., Stanford Univ., Stanford, Calif., 1974.

Burtis, J. W., and R. A. Helliwell, Magnetospheric chorus, occurrence patterns and normalized frequency, Planet. Space Sci., 24, 1007, 1976.

Burton, R. K., and R. E. Holzer, The origin and propagations of chorus in the outer magnetosphere, J. Geophys. Res., 79, 1014, 1974.

Calvert, W., The signature of auroral kilometric radiation on Isis 1 ionogram, J. Geophys. Res., 86, 76, 1981.

Cerisier, J. C., Propagation perpendiculaire au voisinage de la fréquence de la résonance hybride basse, in Plasma Waves in Space and in the Laboratory, vol. 2, pp. 487-521, Edinburgh, University Press, 1970.

Church, S. R., and R. M. Thorne, On the origin of the plasmaspheric hiss: Ray path integrated amplification, J. Geophys. Res., 88, 7941, 1983.

Cornilleau-Wehrlin, N., R. Gendrin, F. Lefeuvre, M. Parrot, R. Grard, D. Jones, A. Bahsen, E. Ungstrup, and W. Gibbons, VLF electromagnetic waves observed onboard GEOS-1, Space Sci. Rev., 22, 371, 1978.

Etcheto, J., R. Gendrin, J. Solomon, and A. Roux, A self-consistent theory of magnetospheric ELF hiss, J. Geophys. Res., 78, 8150, 1973.

Gallagher, D. L., and D. Gurnett, Auroral kilometric radiation: Time-averaged source location, J. Geophys. Res., 84, 6501, 1979.

Gendrin, R., Le guidage des whistlers par le champ magnétique, Planet. Space Sci., 5, 274, 1961.

Goldstein, B. E., and B. T. Tsurutani, Wave normal directions of chorus near the equatorial source region, J. Geophys. Res., 89, 2789, 1984.

Green,J. L., D. A. Gurnett, and S. D. Shawhan, The angular distribution of auroral kilometric radiation, J. Geophys. Res., 82, 1825, 1977.

Gurnett, D. A., and J. L. Green, On the polarization and origin of auroral kilometric radiation, J. Geophys. Res., 83, 689, 1978.

Helliwell, R. A., and U. S. Inan, VLF wave growth and discrete emission triggering in the magnetosphere: A feedback model, J. Geophys. Res., 87, 3537, 1982.

Huang, C. Y., C. K. Goertz, and R. R. Anderson, A theoretical study of plasmaspheric hiss generation, J. Geophys. Res., 88, 7927, 1983.

James, H. G., VLF saucers, J. Geophys. Res., 81, 501, 1976.

James, H. G., Direction of arrival measurements of auroral kilometric radiation and associated ELF data from ISIS 1, J. Geophys. Res., 85, 3367, 1980.

Kennel, C. F., and H. E. Petschek, Limit on stably trapped particle fluxes, J. Geophys. Res., 71, 1, 1966.

Kennel, C. F., and R. M. Thorne, Unstable growth of unducted whistlers propagating at an angle to the geomagnetic field, J. Geophys. Res., 72, 871, 1967.

Koons, H. C., The role of hiss in magnetospheric chorus emissions, J. Geophys. Res., 86, 6745, 1981.

Kurth, W. S., M. M. Baumback, and D. A. Gurnett, Direction-finding measurements of auroral kilometric radiation, J. Geophys. Res., 80, 2764, 1975.

Lagoutte, D., and F. Lefeuvre, Analyse spectrale des composantes d'un champ d'onde électromagnétique se propageant dans un magnétoplasma par un modèle AR vectoriel, paper presented at Neuvième Colloque sur le Traitement du Signal et Ses Applications, Nice, France, May 1983.

Lefeuvre, F., Analyse de champ d'ondes électromagnétiques aléatoires observés dans la magnétosphère à partir de la mesure simultanée de leurs six composantes, thèse de doctorat d'état, univ. of Orléans, Orléans, France, 1977.

Lefeuvre, F., and C. Delannoy, Analysis of a random electromagnetic wave field by a maximum entropy method, Ann. Telecommun., 34, 204, 1979.

Lefeuvre, F., M. Parrot, and C. Delannnoy, Wave distribution functions estimation of VLF electromagnetic waves, J. Geophys. Res., 86, 2359, 1981.

Lefeuvre, F., M. Parrot, L. R. O . Storey, and R. R. Anderson, Wave distribution functions for plasmaspheric hiss observed on-board ISEE-1, Tech. Note LPCE-6, CNRS/Lab. en Phys. et Chim. de l'Environ., Orléans, France, March 1983.

Lefeuvre, F., T. Neubert, and M. Parrot, Wave normal directions and wave distribution functions for ground-based transmitter signals observed on GEOS 1, J. Geophys. Res., 87, 6203, 1982.

Likhter, Ja. I., ELF and VLF noise intensity and spectra in the magnetosphere, in Wave Instabilities in Space Plasmas, edited by P. J. Palmadesso and R. Papadopoulos, p. 3, D. Reidel publishing Company, Dordrecht, 1979.

Rauch, J. L., and A. Roux, Ray tracing of ULF waves in a multicomponent magnetospheric plasma: Consequences for the generation mechanism of ion cyclotron waves, J. Geophys. Res., 87, 8191, 1982.

Roux, A., S. Perraut, J. L. Rauch, C. de Villedary, G. Kremser, A. Korth, and D. T. Young, Wave-particle interactions near ΩH_{e^+} observed on board GEOS 1 and 2, 2, Generation of ion cyclotron waves and heating of He^+ ions, J. Geophys. Res., 87, 8174, 1982.

Russel, C. T., R. E. Holzer, and E. J. Smith, OGO 3 observations of ELF noise in the magnetosphere, 1, Spatial extent and frequency of occurrence, J. Geophys. Res., 74, 755, 1969.

S-300 Experimenters, Measurements of electric and magnetic wave fields and of cold plasma parametres onboard GEOS 1, preliminary results, Planet. Space Sci., 27, 317, 1979.

Storey, L. R. O., and F. Lefeuvre, The analysis of 6-component measurements of a random electromagnetic wave field in a magnetoplasma, I, The direct problem, Geophys. J. R. Astron. Soc., 56, 255, 1979.

Storey, L. R. O., and F. Lefeuvre, The analysis of 6-component measurements of a random electromagnetic wave field in a magnetoplasma, II, The integration kernels, Geophys. J. R. Astron. Soc., 173, 1980.

Taylor, W. L. and S. D. Shawhan, A test of incoherent Cerenkov radiation for VLF hiss and other magnetospheric emissions, J. Geophys. Res., 79, 105, 1974.

Thorne, R. M., Whistler mode propagation off the geomagnetic meridian plane, internal report,

Dep. of Meteorol. Univ. of Calif., Los Angeles, Calif., 1969.

Thorne, R. M., E. J. Smith, R. K. Burton, and R. E. Holzer, Plasmaspheric hiss, J. Geophys. Res., 78, 1581, 1973.

Thorne, R. M., S. R. Church, and D. J. Gorney, On the origin of plasmaspheric hiss: The importance of wave propagation and the plasmapause, J. Geophys. Res., 84, 5241, 1979.

Tsurutani, B. T., E. J. Smith, H. I. West, Jr., and R. M. Buck, Chorus, energetic electrons and magnetospheric substorms, in , Wave Instabilities in Space Plasmas, edited by P. J. Palmadesso and K. Papadopoulos,p.55, D. Reidel publishing company, Dordrecht, 1979.

Tsurutani, B. T., and E. J. Smith, Two types of magnetospheric ELF chorus and their substorm dependences, J. Geophys. Res., 82, 5112, 1977.

R. A. Helliwell, Radioscience Laboratory, Stanford Universitv, Stanford, CA 94305, Telex 348402 STANFRD STNU.

F. Lefeuvre, Laboratoire en Physique et Chimie de l'Environnement, 3A Avenue de la Recherche Scientifique, 45045 Orléans Cedex, France. Telex 760600 CNET RL.

(Received November 21, 1983;
revised February 1, 1985;
accepted February 4, 1985.)